Geometric Acceleration of Complex Chemical Equilibrium Calculations – Performance in Two- to Five-component Systems

Willem A. Roos[a,*], Alfred E.J. Bogaers[b], Johannes H. Zietsman[a,b]

[a] *University of Pretoria, Pretoria, South Africa*
[b] *Ex Mente Technologies, Pretoria, South Africa*

Abstract

Incorporating multicomponent, multiphase, complex chemical equilibrium calculations into process and multiphysics models can provide significant insights into industrial processes that current modelling or measurements cannot. Equilibrium calculations are however, in general, omitted or incorporated in a simplified manner due to their computational expense. Several methods have been developed to accelerate these calculations.

A new accelerator algorithm was developed [1] based on phase diagram geometry, the Gibbs phase rule, and the lever rule to include equilibrium calculations into models more efficiently. This framework of established thermochemical theory provides a sound basis for discretisation and interpolation, and allows the accelerator algorithm to work in systems with any number of components. The work presented here aimed to test accelerator performance and demonstrate that it has the capability of achieving noteworthy levels of acceleration while maintaining acceptable accuracy.

The accelerator was tested on ten 2-component systems, four 3-component systems, a simplified 4-component ilmenite smelting system, and a simplified 5-component iron- and steelmaking system. As the number of system components increased, so did the computational expense of direct equilibrium calculations. This translated to larger acceleration factors for higher-order systems – from 20 in 2-component systems to 1000 in the 5-component system. In a small number of cases it was observed that the acceleration factor was smaller than one during interpolation. This was attributed to slow searching times for suitable interpolation cells from the database.

Phase composition interpolation errors are less than $1 \times 10^{-2}\,\mathrm{mol\,mol^{-1}}$. This translates to an interpolated phase composition being accurate to within 99 % of the calculated composition and results in phase fraction errors of 1×10^{-2} and less. In a very small number of cases the interpolation errors made on physical and thermochemical properties are as high 10 %. This is because system properties are calculated as a phase fraction weighted sum of phase properties and errors made on system properties can therefore become large due to interpolation errors being made twice. However, the majority of errors made on physical and thermochemical properties are in the order of 1 % and less. The level of accuracy achieved by the accelerator algorithm was acceptable for the chosen discretisation tolerances.

Keywords: equilibrium calculations; CALPHAD; acceleration; generic lever rule; Gibbs phase rule; process and multiphysics models

1. Introduction

Incorporating multicomponent, multiphase, high-temperature, complex chemical equilibrium calculations, hereafter simply referred to as equilibrium calculations, into multiphysics and process models, hereafter simply referred to as models, can provide valuable insight into industrial processes that current modelling or measurements cannot. The word "model" in this work is not associated with thermochemical solution models. Equilibrium calculations provide phase fractions, phase compositions, physical properties such as heat capacity and thermochemical properties such as enthalpy as functions of system temperature, pressure, and composition. Some additional material properties that may be required by models are not provided by equilibrium calculations. However, material property models can estimate additional properties such as viscosity, density, thermal and electrical conductivity based on equilibrium calculation results. Although this approach can provide more accurate material properties to models, equilibrium calculations are computationally expensive and are usually omitted or incorporated in a simplified manner. The authors previously reported on mathematical and numerical aspects of equilibrium calculations and their computational expense [2].

As shown in Figure 1, there is a high-order non-linear relationship between a system's number of components and equilibrium calculation computation time. Multiphysics models can have thousands or even millions of mesh cells and an equilibrium calculation may need to

be performed in each cell for every iteration. Multiple iterations are, however, required for convergence and multiple time steps when a transient model is solved. This can also lead to total computation times ranging from days to years. In cases with many system components, mesh cells, iterations, and time steps, direct calculations of equilibrium calculations (direct calculations) can result in infeasible solving times.

The same high-order non-linear relationship between a system's number of components and equilibrium calculation computation time is seen in process models. The difference is that these models do not have mesh cells to consider, but still need to perform many equilibrium calculations when the process is divided into multiple equilibrium reactors [3]. Many calculations can be required to ensure convergence to steady state, and even more so for process simulations with transient models and when these models are used with optimisation routines. Solving times can easily become infeasible.

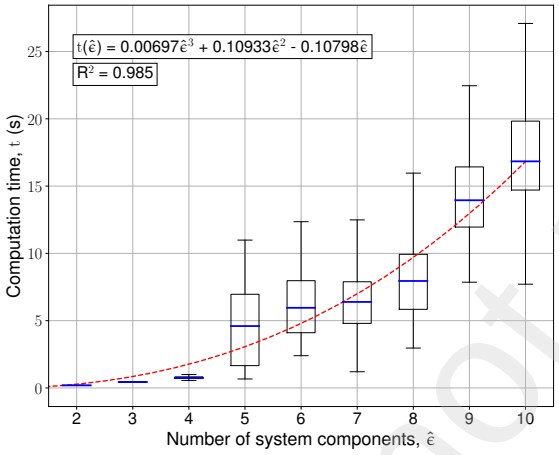

Figure 1: Third-order increase in equilibrium calculation computation time with number of system components. Initial system was Fe-O, and Si, Al, Mg, Ca, N, Mn, Na, K were added. 250 randomly distributed equilibrium calculations per ê-component system. Calculated with ChemAppPy [4], and data from the FToxid database in FactSage 7.2.0. The calculations were done in serial on an Intel Core i7-3770 (4 cores) with a clock speed of 3.4 GHz and had 8 GB of RAM available.

Several methods have been developed to improve the computational efficiency of including equilibrium calculations into models so that more comprehensive simulations can be done in a reasonable time. This includes methods such as creating look-up tables prior to the simulation or during (in-situ), fitting piecewise polynomial functions to thermochemical properties, phase diagram discretisation, sensitivity derivatives, artificial neural networks, and parallelisation. These methods either improve the efficiency of equilibrium calculations or store calculation results for later recall and interpolation, which is less costly than direct calculations. The authors previously reviewed these methods [2].

Conceptually, an equilibrium calculation accelerator, together with data stored in its database, acts as an intermediary between a model and equilibrium calculation software, as illustrated in Figure 2. In this work, the word "database" refers to the collection of calculated thermochemical properties and not to the thermochemical database that contains thermochemical solution models. The accelerator's database can be populated prior to solving the model, or while the model is being solved (in-situ). When possible, the accelerator recalls stored data and uses it in an interpolation scheme to calculate thermochemical properties $\tilde{\mathbf{Y}}^{\sigma}$ rather than performing a more computationally expensive equilibrium calculation to obtain the thermochemical properties $\mathbf{Y}^{\sigma}$ directly.

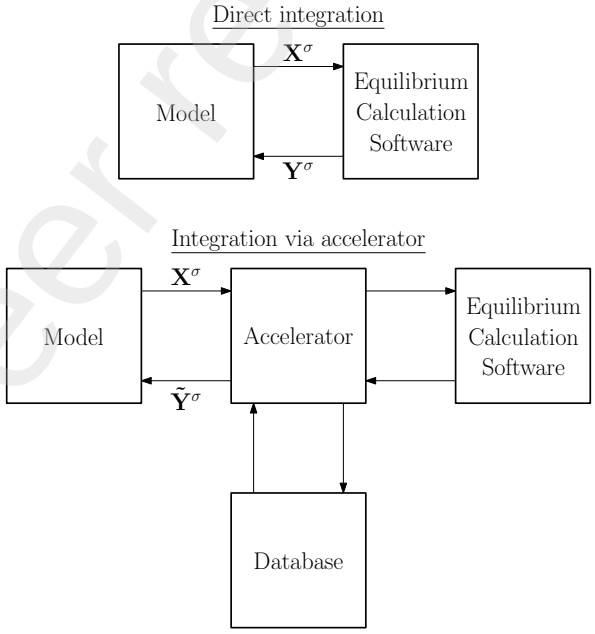

Figure 2: Schematic representation of direct calculation and integration of an accelerator between a model and equilibrium calculation software. Adapted from Zietsman [5]

A new accelerator algorithm was developed by the authors and its performance tested in a number of 2- and 3-component alloy and slag systems [1]. Improvements have since been made on the interpolation algorithm, and the accelerator's capabilities in 2- and 3-component systems are revisited in this work. Phase diagrams and the discretised phase regions could be visualised in 2D and 3D to assist with the verification that the algorithm functioned as intended. Thereafter, the performance of the accelerator was tested in two systems that are related to industrial processes where the inclusion of a large number of equilibrium calculations into models could provide valuable insight. These systems are the simplified 4-component ilmenite smelting system, C–Fe–O–Ti, and the simplified 5-component iron- and steelmaking system, C–Ca–Fe–O–Si. This provides insight into how the accelerator would perform if it was incorporated into

a model of these processes.

A brief background of the developed accelerator and its implementation are presented in Section 2 together with the latest interpolation improvements. The methods used to measure the performance of the accelerator algorithm as well as the conditions under which the tests were performed are discussed in Section 3. The results and findings of the revisited accelerator performance tests in 2- and 3-component systems are presented in Section 4. Results from the performance tests where the accelerator algorithm was applied to two industry-related processes are presented Section 5. Thereafter the concluding remarks are made in Section 6.

2. Accelerator Algorithm

2.1. Brief Background

Based on the initial work done by Zietsman [5] and the lessons learnt from reviewing previous methods of accelerating equilibrium calculations [2], an accelerator algorithm was developed by the authors [1]. The accelerator algorithm performs an equilibrium calculation and stores the calculated equilibrium state $\mathbf{Y}^{\sigma}$ as a tie simplex. The compositions of all stable phases are the vertices of the tie simplex, which are located on the phase region boundaries. Phase properties such as heat capacity and enthalpy are stored with phase compositions.

The Gibbs phase rule is used to determine the number of tie simplices that are required to combine into a discrete portion of the phase region, which is referred to as a phase region cell. This is done in-situ – the phase diagram is only discretised and data stored in those parts of phase regions that are accessed by the model. To control the interpolation accuracy, only tie simplices that are within a specified temperature tolerance $\Delta T^{\mathcal{D}}$ and each phase composition within a composition tolerance $\Delta x_{\epsilon}^{\mathcal{D}}$ can be combined to form a phase region cell.

Interpolation is performed between stored tie simplices of a phase region cell to obtain an interpolated tie simplex that contains the system state where phase compositions and thermochemical properties are required. Thereafter, a generic lever rule is applied on the interpolated tie simplex to determine the interpolated equilibrium state $\tilde{\mathbf{Y}}^{\sigma}$ required by the model.

The accelerator algorithm is strongly based on two elements of basic thermochemical theory; the Gibbs phase rule and lever rule. The reader is referred to [1] for a more detailed explanation of the accelerator algorithm.

2.2. Algorithm Implementation

The algorithm was implemented in Python3 [6], an interpreted programming language. Compiled languages such as C and Fortran would deliver faster solving times, but for development work Python3 enables rapid development of different discretisation, storage and recall, and interpolation routines and sub-routines. The thermochemical software used in the algorithm is ChemAppPy [4] – a package that makes the thermochemical data of ChemApp available in Python3. This made it possible to perform large numbers of equilibrium calculations from within Python3.

The algorithm will be transferred to a compiled language that provides more performance once the initial development stage has been completed. Calculations were performed on a computer with an Intel Core i7-1165G7 CPU with a maximum clock speed of 4.7 GHz and 40 GB of RAM.

2.3. Improvement on Iterative Interpolation Subroutine

The interpolation routine first interpolates towards all the non-compositional potentials of the system, such as temperature and pressure, before interpolating towards the system component chemical potentials. In phase regions where the number of phases equal to the number of independent system components, e.g. 3-phase regions in a 3-component system, a straightforward linear interpolation is performed towards the chemical potentials. In all other phase regions an iterative subroutine is used to interpolate towards the chemical potentials. The reader is referred to [1] for a detailed description of the accelerator interpolation subroutines together with the derivation of the system of non-linear equations employed in the iterative subroutine.

In the original implementation, the system of non-linear equations were solved using the fsolve algorithm from SciPy [7] – a general non-linear equation solver – which proved to be computational expensive because the number of equations were more than the number of unknowns. For this reason, it was decided to change the solution strategy to improve the solution speed by re-casting the system of non-linear equations as a general minimisation problem. The objective function for the minimisation problem was defined as the sum of the squared residual of the non-linear equations. Given the shape of the set of equations, solving the minimisation problem using a gradient-based optimisation algorithm resulted in near quadratic convergence rates, which for the current study was solved using the default BFGS algorithm from SciPy [7].

The original iterative subroutine as implemented in [1] was detrimental to the overall acceleration performed, as reported for 2-phase regions in previously tested 3-component systems. The newly formulated residual minimisation subroutine resulted in notable acceleration now being observed in all phase regions. The interpolation routine's performance could be improved even more by replacing the iterative subroutine with an explicit expression. However, a generic explicit expression that could work in all phase regions in all systems could not be found in literature or derived yet.

3. Approach and Methodology

The methods used to measure the accelerator performance were established before the tests were performed. Thereafter, the conditions under which the performance tests were performed were determined.

3.1. Performance Measurement

The interpolated equilibrium state $\tilde{\mathbf{Y}}^{\sigma}$ consists of the phase compositions $\tilde{\mathbf{x}}_{\epsilon}^{\varphi}$, phase fractions $\tilde{x}_{\varphi}^{\sigma}$, and physical $\tilde{\rho}^{\sigma}$ and thermochemical properties $\tilde{\tau}^{\sigma}$ of the system. The accelerator is not only developed with a reduction in computation time in mind but it has to maintain a degree of accuracy as well. Because linear interpolation is employed in the accelerator, some margin of error is expected, and when quantified, can be measured and compared to direct calculation. The following metrics are used to measure the performance of the accelerator algorithm and quantify the errors made on the different interpolated equilibrium state properties.

3.1.1. Acceleration

The acceleration factor (AF) indicates by what factor the computation time has been improved by the accelerator with respect to direct calculation, and is shown in Equation (1). When the accelerator's computation time Δt(accelerator) is less than direct calculation Δt(direct), the acceleration factor is larger than one – computation time has been accelerated.

$$\mathrm{AF} = \frac{\Delta \mathrm{t(direct)}}{\Delta \mathrm{t(accelerator)}} \tag{1}$$

3.1.2. Phase Characteristics

To calculate the error being made on the composition of phase i, the distance is determined between the phase's composition as determined by the accelerator $\tilde{\mathbf{x}}_{\epsilon}^{\varphi_i}$ and by direct calculation $\mathbf{x}_{\epsilon}^{\varphi_i}$. The distance is calculated with Equation (2). This provides a positive scalar value that expresses the error being made.

$$\mathrm{d}x_{\epsilon}^{\varphi_i} = \mid \tilde{\mathbf{x}}_{\epsilon}^{\varphi_i} - \mathbf{x}_{\epsilon}^{\varphi_i} \mid \tag{2}$$

The difference between the phase fraction of phase i calculated by the accelerator $\tilde{x}_{\varphi_i}^{\sigma}$ and direct calculation $x_{\varphi_i}^{\sigma}$ is determined with Equation (3).

$$\mathrm{d}x_{\varphi_i}^{\sigma} = \tilde{x}_{\varphi_i}^{\sigma} - x_{\varphi_i}^{\sigma} \tag{3}$$

3.1.3. System Properties

To measure the accuracy of extensive thermochemical properties and physical properties, the percentage error between the property calculated by the accelerator and direct calculation, with respect to direct calculation, is determined. The property calculation error for physical properties is shown in Equation (4) and for extensive thermochemical properties in Equation (5). This is done on the system physical and thermochemical properties only in this work.

$$E\rho^{\sigma}(\%) = \frac{\tilde{\rho}^{\sigma} - \rho^{\sigma}}{\rho^{\sigma}} \times 100 \quad \text{where } \rho \in \{C_p\} \tag{4}$$

$$E\tau^{\sigma}(\%) = \frac{\tilde{\tau}^{\sigma} - \tau^{\sigma}}{\tau^{\sigma}} \times 100 \quad \text{where } \tau \in \{H, S, G\} \tag{5}$$

3.2. Test Conditions

For all tests, a composition tolerance $\Delta x_{\epsilon}^{\mathcal{D}}$ of $0.01\,\mathrm{mol\,mol^{-1}}$ was used for all system components, and a temperature tolerance $\Delta T^{\mathcal{D}}$ of 10 K was used as the basis for discretisation.

3.2.1. 2- and 3-component Systems

Accelerator performance was tested in a number of 2- and 3-component alloy and oxide systems, as listed in Table 1. In each system, a total of 200 000 system states $\mathbf{X}^{\sigma}$ were randomly generated within the entire composition range of each system component and within a chosen temperature range. Each randomised system state was provided to the accelerator algorithm to obtain an interpolated equilibrium state $\tilde{\mathbf{Y}}^{\sigma}$ and then a direct calculation was performed for the same system state to obtain the calculated system state $\mathbf{Y}^{\sigma}$ which serves as control. The interpolated equilibrium states $\tilde{\mathbf{Y}}^{\sigma}$ were then compared to the calculated equilibrium states $\mathbf{Y}^{\sigma}$ to evaluate the accuracy of interpolated states.

Table 1: 2- and 3-component systems used to test the accelerator.

Alloy System	Oxide System
Al–Cu	Al_2O_3–CaO
Al–Mn	Al_2O_3–MgO
Al–Zn	Al_2O_3–SiO_2
Fe–C	CaO–SiO_2
Fe–Cr	Al_2O_3–CaO–MgO
Fe–Si	Al_2O_3–CaO–SiO_2
	Al_2O_3–Fe_2O_3–MgO
	Al_2O_3–Fe_2O_3–SiO_2

3.2.2. 4- and 5-component Systems

Accelerator performance was tested for two industrial processes; a simplified 4-component ilmenite smelting system, C–Fe–O–Ti, and a simplified 5-component iron- and steelmaking system, C–Ca–Fe–O–Si. In each system, several temperature and composition ranges were identified that correspond to regions that are encountered in the industry-related process that would most-likely be accessed by a model when the accelerator is incorporated. For each system, a total of 1 000 000 system states $\mathbf{X}^{\sigma}$ were randomly generated from these identified regions. As with the tests performed in 2- and 3-component systems, the interpolated equilibrium states $\tilde{\mathbf{Y}}^{\sigma}$ were compared to the calculated equilibrium states $\mathbf{Y}^{\sigma}$ to evaluate the accuracy of interpolated states.

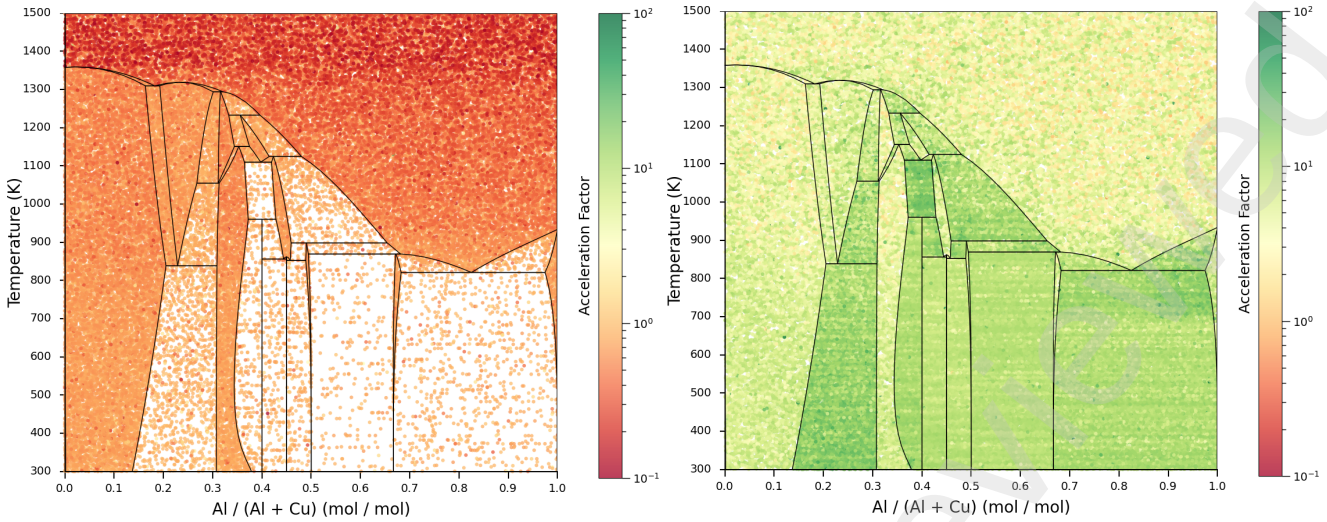

(a) Heat map of discretised states $\mathbf{Y}^{\sigma}$.

(b) Heat map of interpolated states $\tilde{\mathbf{Y}}^{\sigma}$.

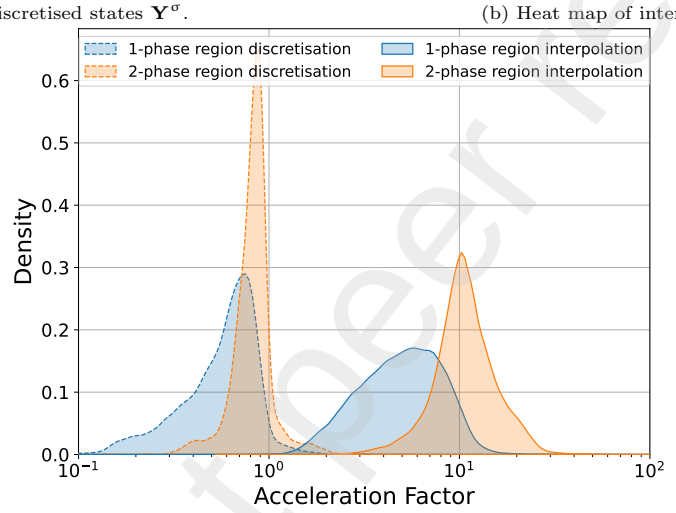

(c) Distributions.

Figure 3: Acceleration factors for the Al–Cu system.

4. Accelerator Algorithm Performance Tests

4.1. Two-component Systems

A temperature range from 300 K up to 100 K above the highest liquidus temperature in the system was used in these tests. The results of the performance tests were very similar amongst all the evaluated 2-component systems and only the Al–Cu system is used to illustrate these findings hereafter.

4.1.1. Acceleration

In Figures 3a and 3b, 2-phase regions show mostly interpolations with large acceleration factors. 1-phase regions show a mix of interpolations with relatively large acceleration factors, and discretisations with acceleration factors of 1 and less. This is due to the size of phase region cells in 1-phase regions being much smaller than in 2-phase regions. Phase region cell size in 1-phase regions are restricted to the specified temperature and composition tolerances, leading to relatively small cells.

On the other hand, although phase region cells in 2-phase regions are also restricted to the temperature tolerance, the phase region cells span the entire width of the phase region – from one phase region boundary to the other – and the composition tolerance only applies to compositions of the phases at the phase region boundaries. This means that fewer direct calculations need to be performed to discretise and cover large portions of 2-phase regions, and a larger number of interpolated equilibrium calculations can be performed much sooner in a simulation.

Figure 3c shows acceleration factors of less than one for the majority of discretisation cases. In addition to performing a direct equilibrium calculation, the resulting tie simplex has to be created and stored, and the database must be interrogated for other tie simplices that can be combined to create a phase region cell.

Despite the need for database searches during inter-

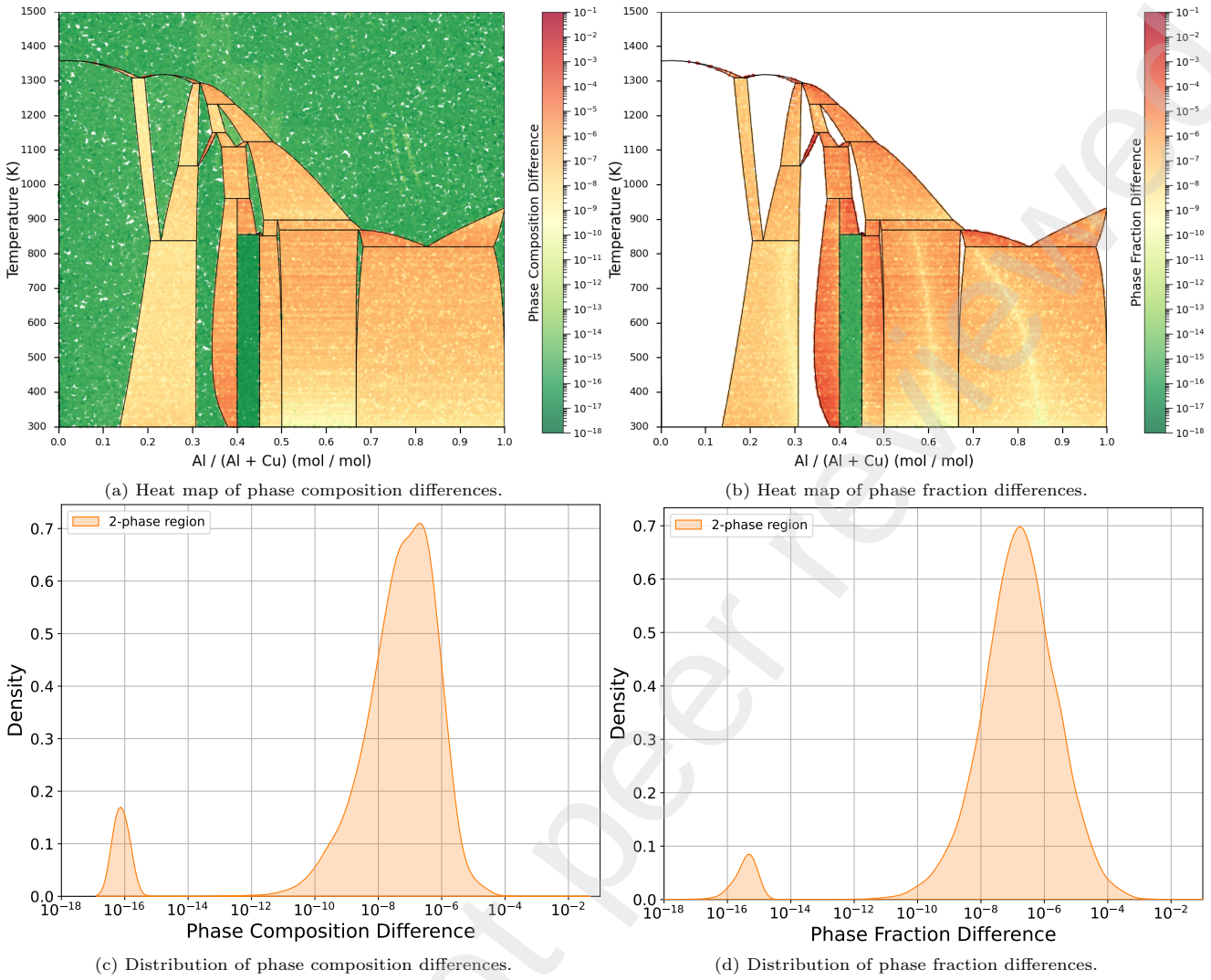

(a) Heat map of phase composition differences.

(b) Heat map of phase fraction differences.

(c) Distribution of phase composition differences.

(d) Distribution of phase fraction differences.

Figure 4: Phase accuracy for the Al−Cu system.

polation, acceleration factors are larger than one in all phase regions, with some calculations showing acceleration factors of more than 10. 2-phase regions gain greater benefits compared to 1-phase regions.

4.1.2. Phase Characteristics

Figure 4a shows small differences in phase compositions for 1-phase regions of about 10^{-16}. Because composition and temperature vary linearly in these regions and linear interpolation is performed, the differences should be equal to zero. The small values are due to floating point machine precision, and the results can be accepted to be exact.

The same applies to 2-phase regions where both phases are pure substances. The phase region boundaries of pure substances are straight vertical lines with constant composition and no interpolation error is made.

In 2-phase regions where at least one solution phase is present, the difference in phase composition is more notable. Phase region boundaries of solution phases vary non-linearly with composition and temperature. When performing linear interpolation on these curved boundaries, errors are made, as shown in the heat maps.

Because phase fractions are calculated from phase compositions, the same trends observed in phase composition differences were also observed in phase fraction differences, as shown in Figure 4b, except for 1-phase regions. Because only one phase is present, the phase fraction in a 1-phase region is always one and the difference between the calculated state and interpolated state is exactly zero. The zero value cannot be plotted on the log scale of the heat map.

Figure 4c shows a narrow distribution in the phase composition difference at 10^{-16} associated with pure substances. There is also a wide distribution between 10^{-12} and 10^{-4} associated with solution phases. The more curved a phase region boundary, the larger the linear interpolation error made, and because there is a large variation in curvature of phase region boundaries in the system, the distribution of phase composition difference

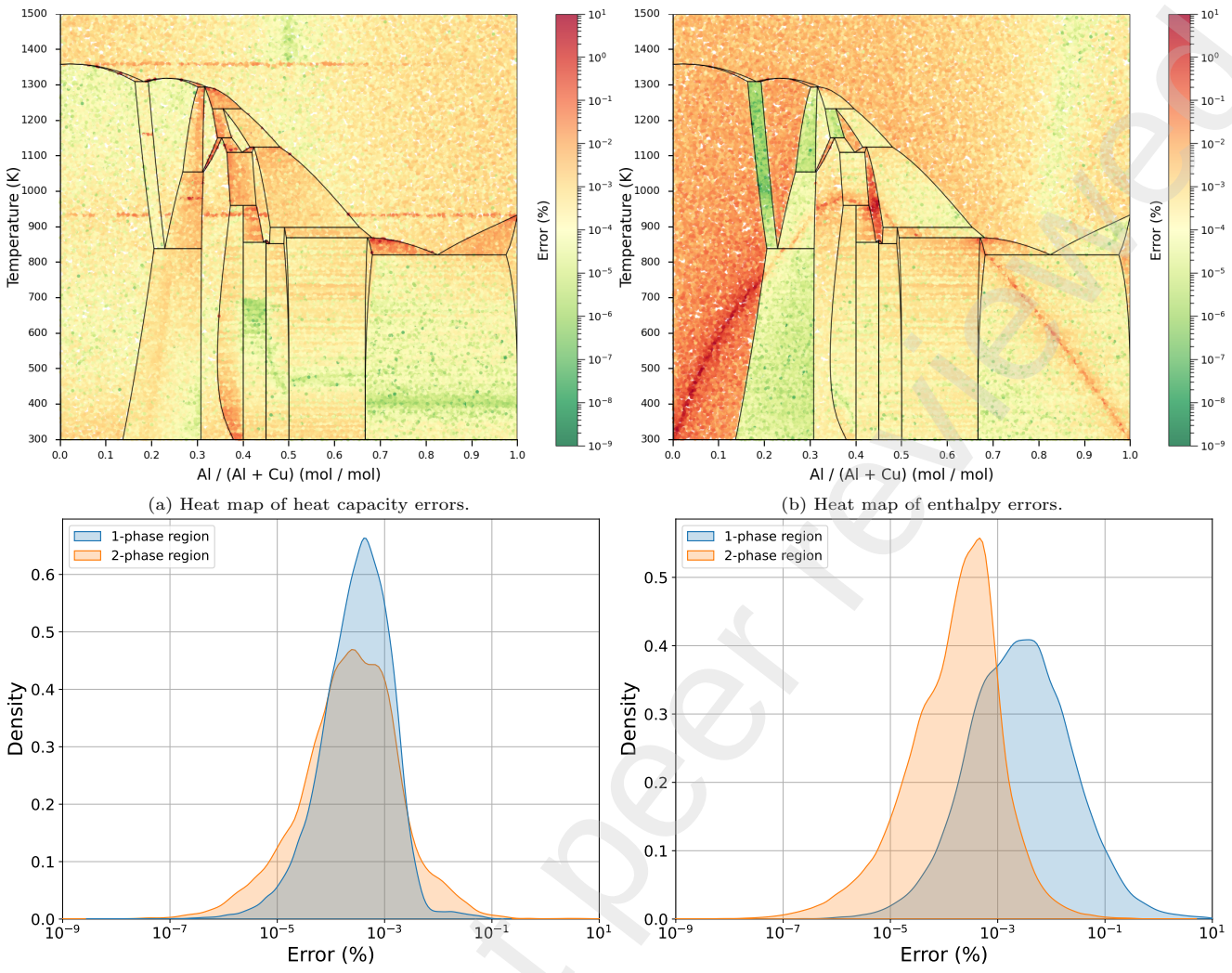

(a) Heat map of heat capacity errors.

(b) Heat map of enthalpy errors.

(c) Distribution of heat capacity errors.

(d) Distribution of enthalpy errors.

Figure 5: Property accuracy for the Al–Cu system.

is wide. Because phase fractions are dependant on phase compositions, the distribution plot of their differences is similar.

4.1.3. System Properties

Physical and thermochemical properties vary non-linearly with composition as well as temperature and linear interpolation errors are expected in all phase regions, which is shown in Figure 5.

System properties are calculated as the phase fraction weighted sum of the phase properties. The error made on these properties can therefore become large as interpolation errors are made twice. Figures 5c and 5d show a wide distribution of errors due to the non-linear property variations and interpolations. Errors for all the properties are in the order of 1 % or less.

4.1.4. Summary of 2-component Systems

Accelerator performance for all the evaluated 2-component systems are summarised in Table 2. Average values for all interpolated equilibrium calculations are reported and separated based on the number of stable phases.

The average acceleration factor for all phase regions in the 2-component systems is larger than one. Significant acceleration was therefore achieved across the entire set of evaluated system states. Some systems show more acceleration than others. This is due to the direct calculation computation time of some systems being longer than others, while the interpolation times remain fairly constant.

2-phase region acceleration factors are higher because when non-compositional potential tie simplices are determined, only one can be created and it automatically becomes the interpolated tie simplex, and no additional interpolation steps are required. In 1-phase regions, two non-compositional potential tie simplices are created and from there an additional interpolation step is required to determine the interpolated tie simplex.

In 2-phase regions, the average differences in phase

Table 2: Summary of algorithm performance in 2-component systems.

System	$\overline{\mathrm{AF}}$	$\overline{\mathrm{d}x_{\epsilon}^{\varphi_i}}$	$\overline{\mathrm{d}x_{\varphi_i}^{\sigma}}$	$\overline{E\rho^{\sigma}}$ (%)		$\overline{E\tau^{\sigma}}$ (%)	
				C_p	H	S	G
1-phase regions							
Al–Cu	5.5			8.9e-04	5.8e-02	2.1e-03	4.0e-03
Al–Mn	7.2			6.5e-04	4.9e-02	1.1e-03	2.8e-03
Al–Zn	5.1			1.2e-03	8.0e-04	2.0e-03	1.8e-03
Fe–C	2.6			1.5e-03	1.6e-03	1.7e-03	3.5e-03
Fe–Cr	4.1			8.6e-03	6.5e-04	1.3e-03	1.4e-03
Fe–Si	11.1			2.3e-02	9.7e-02	1.1e-03	4.2e-03
Al_2O_3–CaO	1.8			7.4e-02	5.7e-04	5.0e-04	2.2e-04
Al_2O_3–MgO	5.0			9.9e-02	3.7e-04	6.4e-04	2.4e-04
Al_2O_3–SiO_2	2.6			1.9e-01	2.0e-04	6.6e-04	1.5e-04
CaO–SiO_2	3.1			3.0e-02	8.1e-04	1.2e-03	2.7e-04
2-phase regions							
Al–Cu	11.5	5.0e-07	6.8e-06	2.9e-02	1.5e-03	6.6e-04	5.3e-04
Al–Mn	13.8	7.8e-07	1.6e-05	3.4e-02	5.5e-03	6.6e-04	4.8e-04
Al–Zn	9.9	1.2e-05	1.2e-05	5.9e-02	4.7e-03	6.4e-04	1.2e-03
Fe–C	4.8	7.6e-08	2.8e-07	1.7e-03	2.3e-03	2.6e-04	8.2e-04
Fe–Cr	10.5	7.2e-06	4.6e-06	3.8e-02	3.7e-03	4.3e-04	1.3e-03
Fe–Si	19.5	1.7e-07	9.2e-07	1.5e-02	1.2e-03	3.5e-04	2.0e-04
Al_2O_3–CaO	3.2	4.0e-08	3.0e-07	2.8e-03	5.5e-06	1.9e-04	2.3e-05
Al_2O_3–MgO	8.5	2.6e-07	7.2e-07	4.3e-02	1.4e-05	7.8e-05	8.3e-06
Al_2O_3–SiO_2	6.2	8.7e-07	1.6e-06	6.2e-03	1.5e-05	8.6e-05	9.6e-06
CaO–SiO_2	5.0	9.3e-08	3.4e-07	4.6e-03	6.4e-06	1.6e-04	2.2e-05

composition and phase fractions are in the order of $10^{-5}\,\mathrm{mol\,mol^{-1}}$ or less. Very small interpolation errors are therefore made. The average errors made on physical and thermochemical properties are in the order of $10^{-2}\,\%$ or less.

The performance of the accelerator algorithm is satisfactory in 2-component systems. Phase composition and fraction differences are acceptable for the chosen temperature and composition tolerances, resulting in acceptable magnitudes of errors made on physical and thermochemical properties. Although the acceleration factor does not seem massive, it should be remembered that direct calculation computation times in 2-component systems are 0.001 s to 0.01 s, which is already fast. In systems with more components and longer direct calculation computation times, which is what this accelerator is being developed for, it is expected to observe much larger acceleration factors.

4.2. Three-component Systems

A temperature range from 1300 K up to 100 K above the highest liquidus temperature in the system was used for these tests. The temperature range was reduced in comparison to the 2-component system tests to maintain a comparable randomised system state density. The results of the performance tests were very similar amongst all 3-component systems and only the Al_2O_3–CaO–SiO_2 system is used to illustrate these findings hereafter.

It is difficult to interrogate heat maps in 3-component systems when they are drawn on the entire 3D phase diagram. Instead, heat maps were drawn on isothermal sections and interrogated. The heat maps illustrated hereafter are shown on the 2000 K isothermal section for all system states within ±5 K.

4.2.1. Acceleration

Figures 6a and 6b show that 3-phase regions have a small number of discretisations with mostly interpolations, while 2-phase regions show more discretisations and fewer interpolations, and 1-phase regions show the most discretisations and the fewest interpolations. This is, as in 2-component systems, due to the size of phase region cells being the smallest in 1-phase regions and increasing in size as the number of stable phases increase.

Figure 6c shows that, as with 2-component systems, the acceleration factor for discretisations is less than one and for interpolations it is larger than one, with some interpolations showing acceleration factors of 10 to 100. Even though the additional interpolation step in 2-phase regions requires iteratively solving a system of non-linear equations, interpolation computation times are shorter than that of the direct calculations and acceleration is still achieved.

4.2.2. Phase Characteristics

Figure 7a shows that all the accessed 3-phase regions have a solution phase (slag) present; hence the average

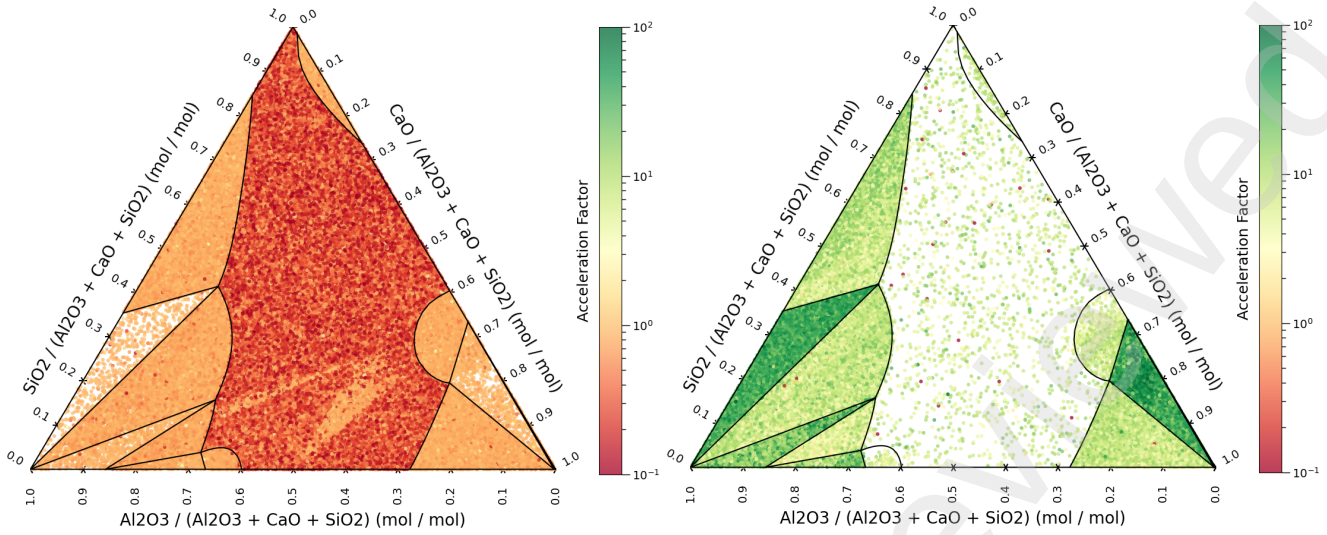

(a) Heat map of discretised states $\mathbf{Y}^{\sigma}$ (2000 K isotherm ±5 K).

(b) Heat map of interpolated states $\tilde{\mathbf{Y}}^{\sigma}$ (2000 K isotherm ±5 K).

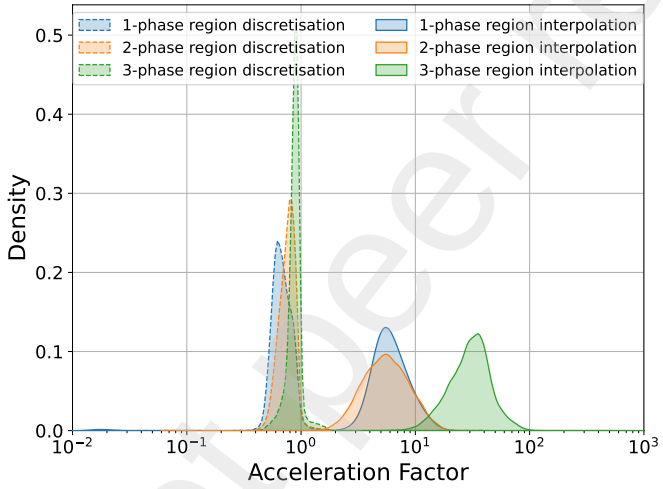

(c) Distributions.

Figure 6: Acceleration factors for the $Al_2O_3-CaO-SiO_2$ system.

phase composition difference at the system states not being as low as 10^{-16} as when only pure substances are present. The phase composition difference in 2-phase regions are relatively large, but as in the 2-component system tests, its is attributed to the curvature of the solution phase's boundary and interpolation errors being made on the phase composition. Because phase fractions are dependant on phase compositions, the same trends observed with differences in phase compositions were observed with differences in phase fractions.

A patch of phase composition and fraction differences are seen in the 1-phase region that seem out of place. These are system states that are found in a 2-phase region below the 2000 K isothermal section but is within the ±5 K range.

Figure 7c shows a narrow distribution in the phase composition difference at 10^{-16} associated with pure substances. There is also a wide distribution between 10^{-12} and 10^{-2} associated with the solution phases. Phase fractions are dependant on phase compositions, and therefore similar trends observed with differences in phase compositions were observed with differences in phase fractions.

4.2.3. System Properties

Physical and thermochemical properties vary non-linearly with composition as well as temperature and linear interpolation errors are expected in all phase regions. Figure 8 shows that not only are interpolation errors made on the phase properties but also the phase fractions. System properties are determined by the phase fraction weighted sum of the phase properties, therefore, the error made on the system properties can become large as interpolation errors are made twice. Errors made on all the properties are in the order of 1 % or less with a small number of errors made on heat capacity between 1 % to 10 % in 2-phase regions.

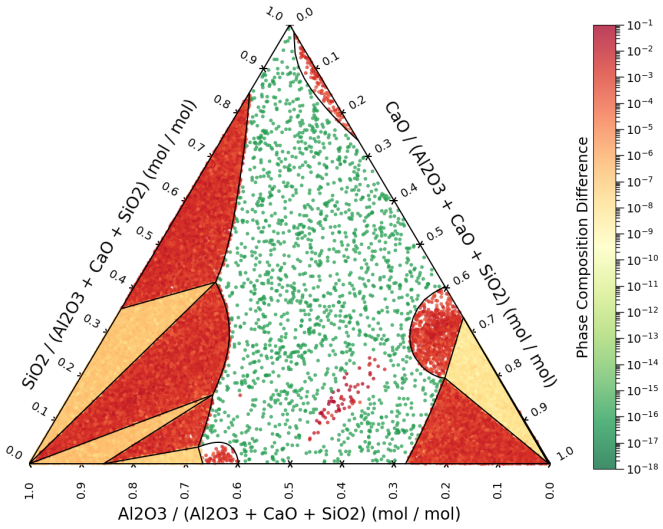

(a) Heat map of phase composition differences (2000 K isotherm ±5 K).

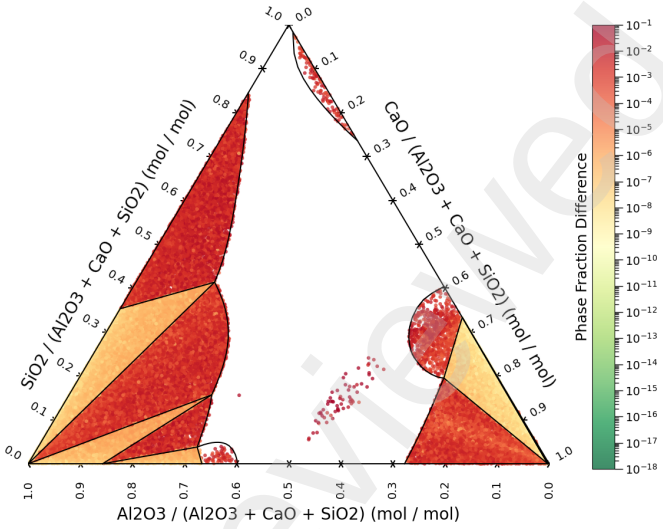

(b) Heat map of phase fraction differences (2000 K isotherm ±5 K).

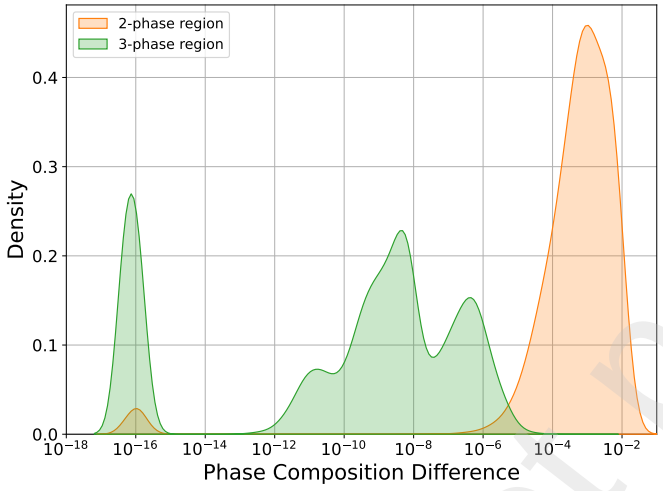

(c) Distribution of phase composition differences.

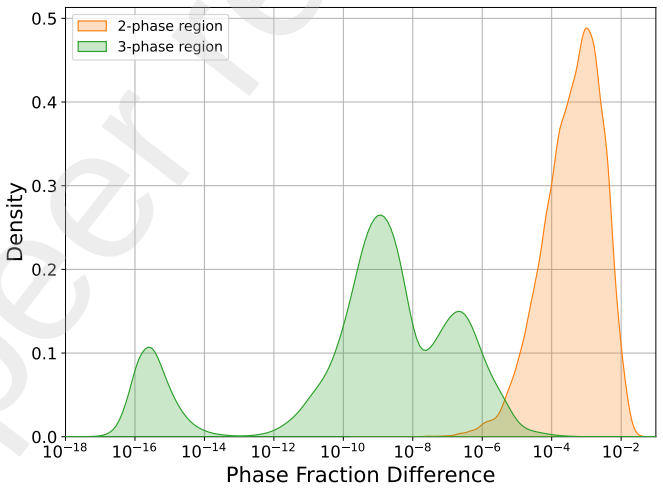

(d) Distribution of phase fraction differences.

Figure 7: Phase accuracy for the Al_2O_3–CaO–SiO_2 system.

4.2.4. Summary of 3-component Systems

Accelerator performance for all the evaluated 3-component systems are summarised in Table 3. The average values for all interpolated equilibrium calculations are reported and separated based on the number of stable phases.

The average acceleration factor for all phase regions in the 3-component systems are larger than one – acceleration was achieved across the set of system states that were evaluated. It can be seen that thee-phase regions' acceleration factors are the highest because when non-compositional potential tie simplices are determined, only one can be created and it automatically becomes the interpolated tie simplex – no additional interpolation steps are required. This is always the case in phase regions where the number of system components $\hat{\varepsilon}$, number of system compositional constrains $\hat{\zeta}^{\sigma}$, and number of phases $\hat{\varphi}$ are in the relation $\hat{\varepsilon} - \hat{\zeta}^{\sigma} = \hat{\varphi}$; 2-phase regions in 2-component systems, 3-phase regions in 3-component systems, etc. In 1- and 2-phase regions, multiple non-compositional potential tie simplices are created and from there an additional interpolation step is required to determine the interpolated tie simplex. Even though this additional step require iteratively solving a system of non-linear equations, the interpolated equilibrium state calculation times were shorter than that of the calculated equilibrium state and acceleration was still achieved. As in 2-component systems, some 3-component systems show more acceleration than others seeing that the direct calculation computation time of some systems being longer than others.

In 2-phase regions, phase composition differences are in the order of 10^{-3} mol mol^{-1} or less and phase fraction differences are in the order of 10^{-3} or less. In the 3-phase regions, phase composition differences are in the order of 10^{-2} mol mol^{-1} and phase fraction differences are in the order of 10^{-2} or less. Overall, the errors made on physical and thermochemical properties are in the order of 10^{-2} %

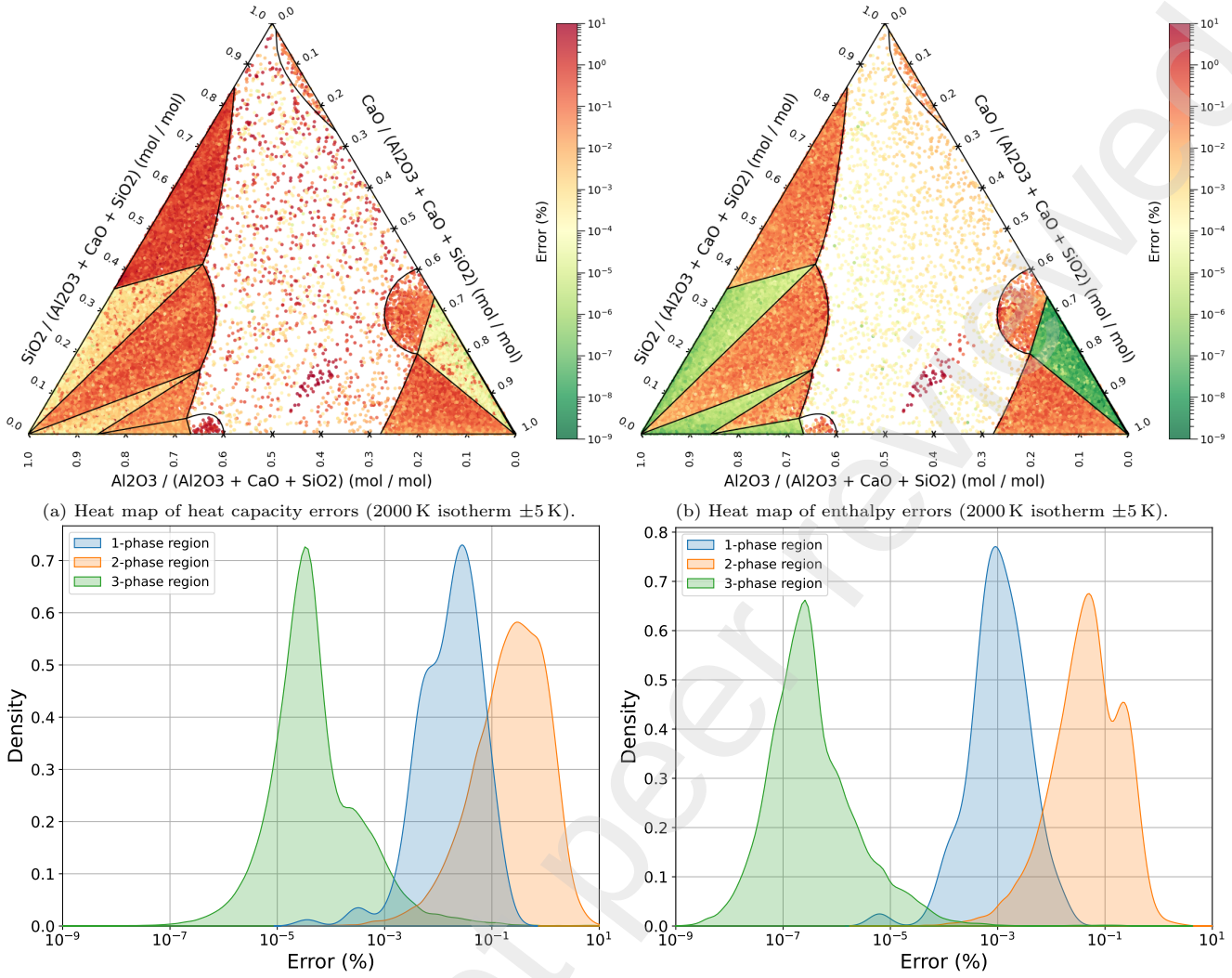

(a) Heat map of heat capacity errors (2000 K isotherm ±5 K).

(b) Heat map of enthalpy errors (2000 K isotherm ±5 K).

(c) Distribution of heat capacity errors.

(d) Distribution of enthalpy errors.

Figure 8: Property accuracy for the $Al_2O_3-CaO-SiO_2$ system.

or less.

The algorithm performance is satisfactory in 3-component systems. The phase composition and fraction differences are acceptable for the chosen temperature and composition tolerances, resulting in acceptable magnitudes of errors made on physical and thermochemical properties. A notable acceleration in equilibrium calculation computation time is already observed in 3-component systems and even larger acceleration factors are expected in systems with more components.

5. Application to Industrial Processes

Accelerator performance was tested on two systems that are related to industrial processes where the inclusion of a large number of equilibrium calculations into models could provide valuable insight. These are a simplified 4-component ilmenite smelting system, C–Fe–O–Ti, and a simplified 5-component iron- and steelmaking system, C–Ca–Fe–O–Si. This provides insight into how the accelerator would perform if it was incorporated into models of these processes.

Exact temperature and composition ranges that will be encountered when the accelerator is included into the models are not known, and may also not be constant during an entire set of simulations, but wide expected ranges were estimated. The purpose of these tests are not to replicate or emulate the inclusion of the accelerator into these models, but rather test the accelerator's performance in multiple phase regions within temperature and compositional ranges that could be expected for these processes.

5.1. Simplified Ilmenite Smelting System

The ilmenite smelting process is a step in the upgrading of TiO_2-containing minerals to TiO_2 pigment and Ti metal [8]. Minerals such as rutile (nominally TiO_2), ilmenite (nominally $FeTiO_3$), leucoxene (naturally upgraded ilmenite to a higher TiO_2 content), and zircon

Table 3: Summary of algorithm performance in 3-component systems.

System	$\overline{\mathrm{AF}}$	$\overline{\mathrm{d}x_{\epsilon}^{\varphi_i}}$	$\overline{\mathrm{d}x_{\varphi_i}^{\sigma}}$	$\overline{E\rho^{\sigma}}$ (%)	$\overline{E\tau^{\sigma}}$ (%)		
				C_p	H	S	G
1-phase regions							
$Al_2O_3-CaO-MgO$	4.8			6.2e-03	1.4e-04	2.4e-03	7.3e-04
$Al_2O_3-CaO-SiO_2$	6.4			1.8e-02	2.0e-03	6.3e-03	6.4e-04
$Al_2O_3-Fe_2O_3-MgO$	6.3			2.1e-03	1.7e-04	2.2e-03	4.9e-04
$Al_2O_3-Fe_2O_3-SiO_2$	13.6			1.5e-04	4.7e-04	4.1e-03	1.3e-03
2-phase regions							
$Al_2O_3-CaO-MgO$	3.9	5.4e-03	2.7e-03	2.9e-02	1.1e-01	2.7e-02	2.8e-02
$Al_2O_3-CaO-SiO_2$	6.3	2.0e-03	1.5e-03	2.8e-02	8.3e-02	2.4e-02	2.2e-02
$Al_2O_3-Fe_2O_3-MgO$	9.7	2.0e-03	1.2e-03	2.7e-02	1.1e-01	1.8e-02	2.1e-02
$Al_2O_3-Fe_2O_3-SiO_2$	63.6	1.9e-03	1.2e-03	1.8e-02	8.7e-02	1.6e-02	1.9e-02
3-phase regions							
$Al_2O_3-CaO-MgO$	20.2	5.0e-02	1.2e-02	2.0e-04	9.4e-06	1.7e-05	5.5e-06
$Al_2O_3-CaO-SiO_2$	34.0	1.7e-07	1.1e-06	4.6e-04	1.6e-04	3.0e-05	1.5e-06
$Al_2O_3-Fe_2O_3-MgO$	89.6	3.2e-01	1.1e-01	1.7e-03	1.4e-05	3.0e-05	6.8e-06
$Al_2O_3-Fe_2O_3-SiO_2$	86.4	4.4e-02	1.4e-02	2.8e-05	5.6e-07	1.8e-05	5.8e-06

(nominally $ZrSiO_4$) are often found together in sand-type deposits, collectively referred to as heavy minerals. Ilmenite is also found in hard rock deposits with much lower concentrations of other heavy minerals.

The purpose of the smelting process is to upgrade the ilmenite, whether separated from the mineral sands or as ore from the hard rock deposits, to a slag [8] with high TiO_2 concentration. The tapped slag is either granulated, or cast into large blocks and then crushed and milled. The high-TiO_2 slag in particulate form is used as a feedstock to produce pigment or titanium metal through additional processes.

The alloy product from the smelting furnace is typically iron with 2 % C [8]. Once the alloy is tapped from the smelting furnace, it is refined to increase the C content and decrease the S content. The high-C alloy is then cast into pigs and distributed to other industries.

A key feature of ilmenite smelting is that the corrosive high-TiO_2 slag cannot be contained through direct contact with any available refractory materials. A layer of slag must be frozen onto the furnace sidewall for safe slag bath containment; this solid layer is known as a slag freeze lining. Growth and melting of the freeze lining involves an intricate thermochemical process influenced by fluid flow and heat transfer in the slag bath, heat transfer through the sidewall, and changes in liquid slag composition.

Comprehensive multiphysics models of the ilmenite smelting process, including its thermochemical interactions between slag bath and freeze lining, are needed to improve the understanding of this challenging high-temperature process. This will allow the design of more stable, robust, and efficient smelting furnaces, and the development of improved operating strategies and control systems, all of which will yield both economic and sustainability benefits. Such models are currently infeasible due to the computational expense of direct equilibrium calculations.

5.1.1. Test Conditions

Because of the high operating temperatures of the alloy and slag baths, the accelerator algorithm was tested from 1500 K to 2100 K. Four regions of interest in the

Table 4: Mass fraction ranges of phase constituents and corresponding system component mole fraction ranges for regions of interest in the ilmenite smelting system tests.

Phase Const.	Mass fraction ($g\,g^{-1}$) Min.	Max.	System Comp.	Mole fraction ($mol\,mol^{-1}$) Min.	Max.
Alloy bath					
C	0.00	0.04	C	0.00	0.16
Fe	0.94	1.00	Fe	0.80	1.00
O	0.00	0.01	O	0.00	0.03
Ti	0.00	0.01	Ti	0.00	0.01
Slag bath					
FeO	0.15	0.20	C	0.00	0.00
TiO_2	0.55	0.60	Fe	0.06	0.08
Ti_2O_3	0.20	0.30	O	0.62	0.64
			Ti	0.29	0.32
Reduction zone					
C	0.08	0.12	C	0.18	0.26
$FeTiO_2$	0.65	0.90	Fe	0.12	0.19
Fe_2O_3	0.00	0.14	O	0.44	0.50
TiO_2	0.00	0.15	Ti	0.13	0.18
Alloy and slag bath interface					
C	0.00	0.02	C	0.00	0.08
Fe	0.46	0.50	Fe	0.41	0.55
FeO	0.07	0.10	O	0.30	0.34
TiO_2	0.27	0.31	Ti	0.14	0.18
Ti_2O_3	0.09	0.15			

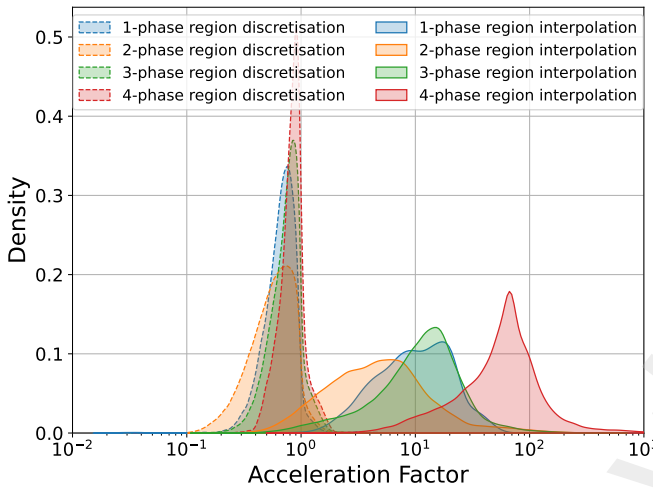

(a) Acceleration factor.

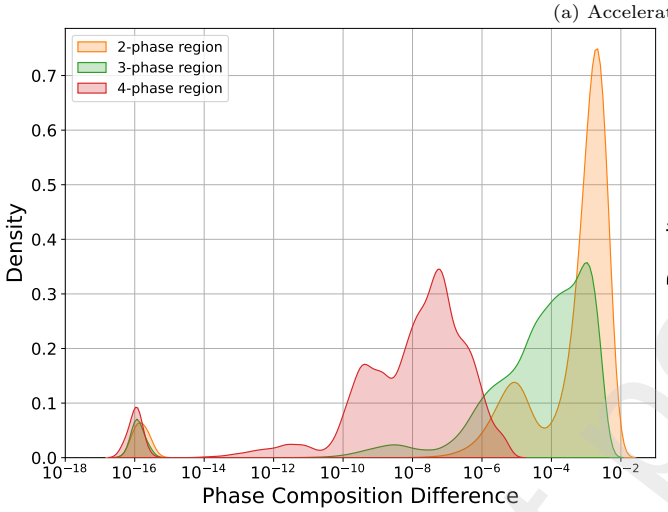

(b) Phase composition differences.

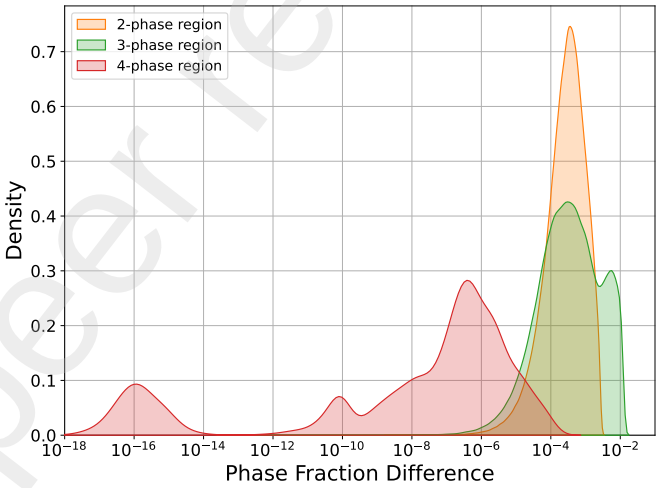

(c) Phase fraction differences.

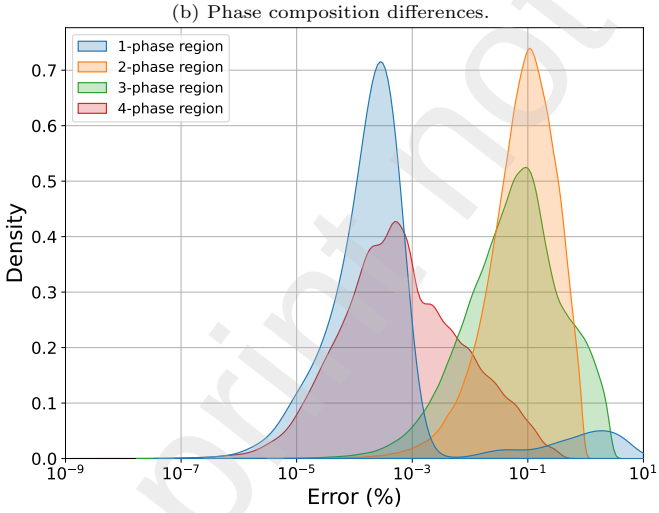

(d) Heat capacity errors.

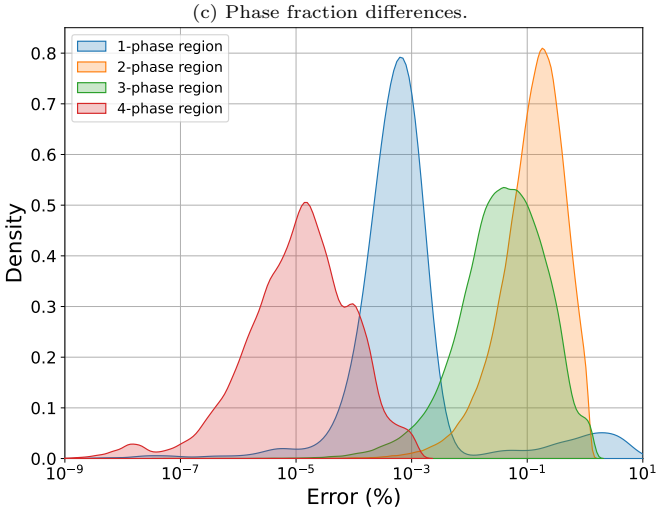

(e) Enthalpy errors.

Figure 9: Accelerator algorithm performance for the simplified ilmenite smelting system.

ilmenite smelting system were investigated with ranges of average compositions identified from literature; 1) the alloy bath [8, 9], 2) the slag bath [8, 9, 10, 11], 3) the reduction zone where ilmenite feedstock [8, 10] and reducing agents are introduced into the furnace in ratios identified from [11], and 4) the interface between the slag and alloy bath as a 1:1 mass-based ratio between the alloy and slag bath. The mass fraction and corresponding

system component mole fraction ranges for the four regions are shown in Table 4.

5.1.2. Results

As was the case for 2- and 3-component systems, Figure 9a shows the acceleration factor to be smaller than one during discretisation for the majority of cases. In a small number of cases, the acceleration factor during the discretisation routine was found to be larger than one. This was simply attributed to the direct calculation taking notably more iterations to determine the equilibrium state in comparison to the equilibrium calculation performed by the discretisation routine.

Even though database searches and frequent iterative calculations are performed during interpolation, the majority of acceleration factors for all phase regions are larger than one. Acceleration factors in the order of 100 and as high as 1000 are achieved in 4-phase regions. In a small number of cases, the acceleration factor for interpolation was smaller than one, which is attributed to a slow searching time for a suitable phase region cell from the database.

Figure 9b shows that the difference in phase composition of 2- and 3-phase regions are in the order of 10^{-2} and less whereas with 4-phase regions the difference is in the order of 10^{-5} and less. The same trend was observed with the phase fraction differences seeing that it is dependent on the interpolated phase compositions.

System properties are determined by the phase fraction weighted sum of the phases' properties, therefore, the error made on the system properties can become large as interpolation errors are made two-fold, as indicated in Figures 9d and 9e. The majority of the errors made on all the properties are in the order of 1 % and less for all phase regions, apart from 1-phase regions that show a small number of errors made in the order of 1 % to 10 %.

5.2. Simplified Iron- and Steelmaking System

Iron- and steelmaking is one of the most CO_2-intensive industries [12] and accounts for 6 % to 9 % of global CO_2 emissions [13]. Regulations have been imposed to reduce emissions, which is leading to the development of new and alternative processes and technologies, some of which substitute carbon with natural gas and hydrogen as reducing agents and utilise renewable energy sources [12].

With stringent deadlines by when emissions have to be reduced and new processes be implemented, there is limited time to build pilot plants to test newly developed processes and even less time for demonstration plants. There is, however, time to build models and use them to rapidly investigate multiple new process concepts, weed out concepts that do not meet requirements, and optimise feasible concepts before new industrial plants are built.

Iron- and steelmaking processes can consist of many system components – in excess of 15 – and this is too many to test the accelerator algorithm with at this stage. However, some preliminary models of the processes can be modelled with a simplified iron- and steelmaking system, C–Ca–Fe–O–Si, and is fitting to perform tests with. Efficient inclusion of equilibrium calculations into multiphysics models of simplified iron- and steelmaking processes can enhance our ability to investigate and develop new process technologies. The slag and alloy baths are of interest as this is where reduction and oxidation processes occur and gas is formed.

5.2.1. Test Conditions

Because of the high temperatures associated with the alloy and slag baths, it was decided to test the accelerator algorithm in the simplified iron- and steelmaking system over a temperature range from 1500 K to 2100 K. Three regions of interest were investigated in the ironmaking stage of the process associated with the blast furnace with ranges of average compositions identified from literature; 1) the alloy bath [14], 2) the slag bath [14, 15, 16], and 3) the reduction zone where iron ore [17, 18] are mixed with reducing agents in ratios identified from [18]. The mass fraction and corresponding system component mole fraction ranges for these three regions are shown in Table 5.

Table 5: Mass fraction ranges of phase constituents and corresponding system component mole fraction ranges for regions of interest in the simplified ironmaking system tests.

Phase	Mass fraction ($g\,g^{-1}$)		System	Mole fraction ($mol\,mol^{-1}$)	
Const.	Min.	Max.	Comp.	Min.	Max.
Alloy bath					
C	0.03	0.05	C	0.12	0.19
Ca	0.00	0.01	Ca	0.00	0.01
Fe	0.91	0.97	Fe	0.74	0.87
O	0.00	0.01	O	0.00	0.03
Si	0.00	0.02	Si	0.00	0.04
Slag bath					
CaO	0.45	0.65	C	0.00	0.00
FeO	0.00	0.02	Ca	0.19	0.28
SiO_2	0.35	0.54	Fe	0.00	0.01
			O	0.57	0.60
			Si	0.14	0.21
Reduction zone					
C	0.19	0.25	C	0.19	0.43
CaO	0.07	0.10	Ca	0.02	0.05
FeO	0.00	0.01	Fe	0.16	0.22
Fe_2O_3	0.64	0.67	O	0.34	0.48
SiO_2	0.09	0.13	Si	0.03	0.06

Three additional regions of interest were investigated in the steelmaking stage of the process associated with the basic oxygen furnace with ranges of average compositions identified from literature; 1) the alloy bath [19], 2) the slag bath [19, 20, 21, 22], and 3) the oxidation zone

where hot metal from the blast furnace, scrap iron and steel, and fluxing agents are introduced into the furnace in close proximity to an oxygen lance, with average compositions and mass ratios identified from [19]. The mass fraction and corresponding system component mole fraction ranges for these three regions are shown in Table 6.

Table 6: Mass fraction ranges of phase constituents and corresponding system component mole fraction ranges for regions of interest in the simplified steelmaking system tests.

Phase	Mass fraction ($g\,g^{-1}$)		System	Mole fraction ($mol\,mol^{-1}$)	
Const.	Min.	Max.	Comp.	Min.	Max.
Alloy bath					
C	0.00	0.03	C	0.00	0.12
Ca	0.00	0.01	Ca	0.00	0.1
Fe	0.97	1.00	Fe	0.88	1.00
O	0.00	0.01	O	0.00	0.03
Si	0.00	0.01	Si	0.00	0.02
Slag bath					
CaO	0.40	0.55	C	0.00	0.00
FeO	0.05	0.10	Ca	0.20	0.28
Fe_2O_3	0.15	0.30	Fe	0.09	0.15
SiO_2	0.10	0.20	O	0.54	0.57
			Si	0.05	0.09
Oxidation zone					
C	0.00	0.04	C	0.00	0.16
Fe	0.91	1.00	Ca	0.00	0.04
Si	0.00	0.01	Fe	0.76	1.00
CaO	0.00	0.04	O	0.00	0.04
			Si	0.00	0.02

5.2.2. Results

Figure 10a shows that, as with the ilmenite smelting system, the acceleration factor is mostly smaller than one during the discretisation routine and mostly larger than one during the interpolation routine.

It can be seen that during the discretisation of 1-phase regions, some acceleration factors are as small as 0.1. This is due to database searches for applicable tie simplices to construct new phase region cells. As mentioned before, phase region cells in 1-phase regions are the smallest and requires the most tie simplices to construct a phase region cell, and therefore need much more tie simplices to be generated, and searched through. As the number of stored tie simplices increase, so does the cost of the search routine. This becomes less problematic as the number of phases increase.

During the interpolation routines, acceleration factors in the order of 100 and as high as 1000 are achieved with the accelerator in 5-phase regions. In a small number of cases, the acceleration factor during the interpolation routine was slightly smaller than one and was attributed to a slow searching time for a suitable phase region cell from the database.

Figure 10b shows that the difference in phase composition of 2- to 5-phase regions are in the order of $1 \times 10^{-2}\,mol\,mol^{-1}$ and less. Differences in the order of $10^{-16}\,mol\,mol^{-1}$ are associated with errors made on the compositions of pure substances. The same trend was observed with the phase fraction differences seeing that it is dependent on the interpolated phase compositions.

Figures 10d and 10e show again that the error made on the system properties can become large. The majority of the errors made on all the properties are in the order of 1 % and less for all phase regions. However, a small number of interpolations performed resulted in errors made on properties in the order of 1 % to 10 %.

6. Conclusion

The accelerator algorithm's performance was tested on ten 2-component, four 3-component systems, a simplified 4-component ilmenite smelting system, and a simplified 5-component iron- and steelmaking system.

1-phase regions have the lowest ratio between the number of interpolations and number of discretisations. As the number of stable phases increases, so does the number of interpolations, along with a decrease in the number of discretisations. This is because the size of phase region cells produced through discretisation is smallest in 1-phase regions and the size increases with the number of stable phases. These larger cells in regions with more stable phases are accessed more regularly for interpolation, which decreases the need for discretisation over large portions of a phase diagram.

As the number of system components increases, so does the computational expense of direct equilibrium calculations. This translates to larger acceleration factors for larger numbers of system components – from acceleration factors as high as 20 in 2-component systems to 1000 in the 5-component system. In a small number of cases the acceleration factor during interpolation was smaller than one, which is attributed to slow searching times for a suitable phase region cell from the database. During discretisation of 1-phase regions in the 5-component system, some acceleration factors were as small as 0.1, which is attributed to database searches for tie simplices to construct new phase region cells. The accelerator algorithm's acceleration performance can be improved by implementing it in a compiled language such as C or Fortran, and using a more performant database system. For this stage of development the acceleration portion of the performance requirement is satisfied.

Interpolation errors made on phase compositions are in the order of $10^{-2}\,mol\,mol^{-1}$ and less and difference in phase fractions are in the order of 10^{-2} and less. This would translate to an interpolated phase composition being accurate to within 99 % of the calculated phase composition, which is satisfactory for this portion of the performance requirement. Although property errors as

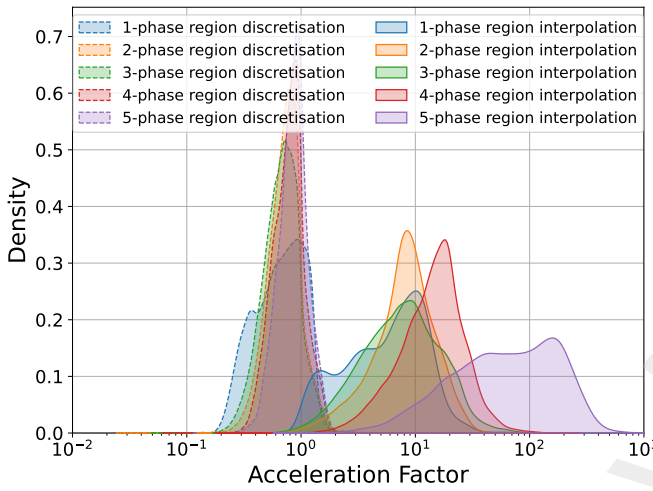

(a) Acceleration factor.

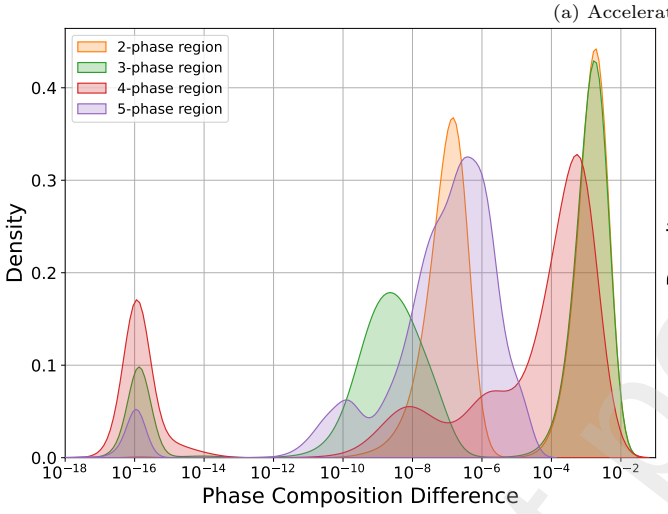

(b) Phase composition differences.

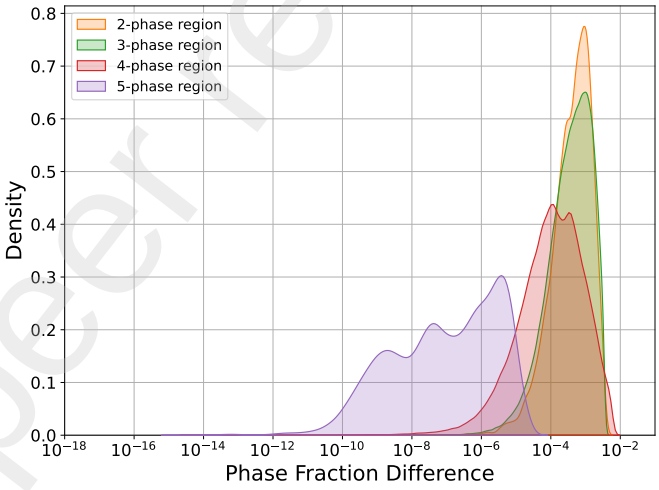

(c) Phase fraction differences.

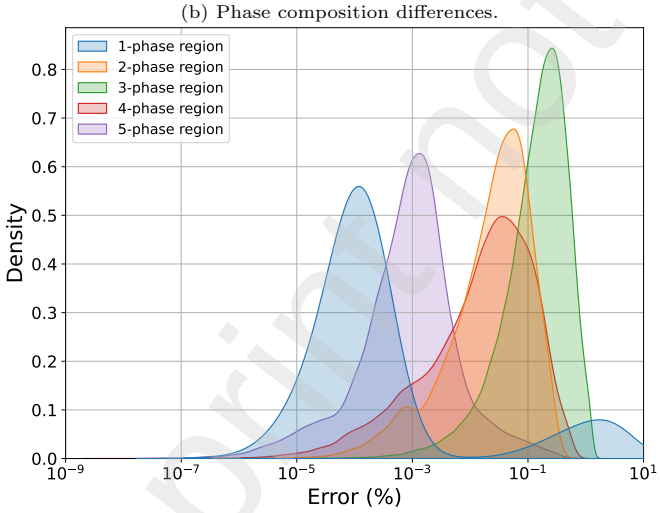

(d) Heat capacity errors.

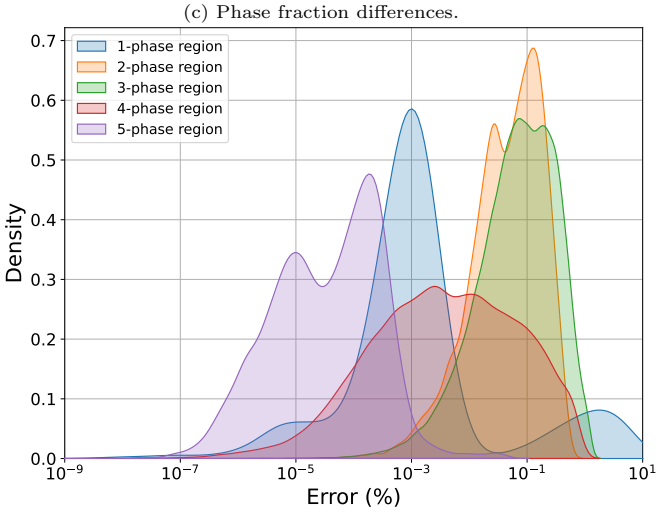

(e) Enthalpy errors.

Figure 10: Accelerator algorithm performance for the simplified iron- and steelmaking system.

high as 10 % are not desired, the accuracy of the majority of property errors were in the order of 1 % and less, which, for this stage of development, satisfies the accuracy portion of the performance requirement. Accuracy can be improved by reducing temperature and compositional tolerances; smaller phase region cells would lead to smaller discretisation steps of phase region boundaries and reduce interpolation errors.

The accelerator algorithm was developed to be generic – to be used with systems with any number of components – by basing it on sound thermochemical principles that scales to any system size. From the performance tests performed, it was demonstrated that the accelerator algorithm has potential of achieving noteworthy levels of acceleration while maintaining acceptable accuracy. There is still room for improving the algorithm, and further development will be done. The next steps, though, will focus on implementing it in a compiled language and using a more suitable database package so that it can be integrated into process and multiphysics models for practical interest to industry.

Declaration of Competing Interest

The authors declare that they have no known competing financial interests or personal relationships that could have appeared to influence the work reported in this paper.

Acknowledgements

The authors would like to thank Ex Mente Technologies for financial support, as well as Glencore through their funding of the Chair in Pyrometallurgical Modelling at the University of Pretoria.

Nomenclature

Thermochemical System Objects

Identifier	Count	
σ		the system
ε	$\hat{\varepsilon}$	system component
ζ^{σ}	$\hat{\zeta}^{\sigma}$	system compositional constraint
ϵ	$\hat{\epsilon}$	independent system component
φ	$\hat{\varphi}$	phase

Compositional Quantities

Scalar	Array	
n	$\mathbf{n}$	amount (mol)
x	$\mathbf{x}$	amount fraction ($\mathrm{mol\,mol^{-1}}$)

Non-compositional Potentials

T	Temperature (K)
p	Pressure (Pa)

Thermochemical Quantities

τ	thermochemical quantity identifier
$\hat{\tau}$	number of thermochemical quantities
T	$\{\bar{V} \quad \bar{H} \quad \bar{S} \quad \bar{G}\}$ set
$\bar{V}$	molar volume ($\mathrm{m^3\,mol^{-1}}$)
$\bar{H}$	molar enthalpy ($\mathrm{J\,mol^{-1}}$)
$\bar{S}$	molar entropy ($\mathrm{J\,K^{-1}\,mol^{-1}}$)
$\bar{G}$	molar Gibbs energy ($\mathrm{J\,mol^{-1}}$)

Physical Properties

ρ	physical property identifier
$\hat{\rho}$	number of physical properties
P	$\{\bar{C}_p \quad \ldots \quad \rho_{\hat{\rho}}\}$ set
$\bar{C}_p$	molar heat capacity at constant pressure ($\mathrm{J\,K^{-1}\,mol^{-1}}$)
ρ	mass density ($\mathrm{kg\,m^{-3}}$)
μ	viscosity (P)
κ	thermal conductivity ($\mathrm{W\,m^{-1}\,K^{-1}}$)

Thermochemical Data Structures

base notation

$\mathbf{X}$		specified state (sp., independent)
$\mathbf{Y}$	$\tilde{\mathbf{Y}}$	equilibrium state (eq., dependent)

Column 1: directly calculated values

Column 2: interpolated equilibrium values indicated with tilde

Interpolated values in arrays only apply to interpolated data structures.

E.g $\tilde{\mathbf{x}}_{\epsilon}^{\varphi_i}$ applies to $\tilde{\mathbf{Y}}^{\varphi_i}$, and $\mathbf{x}_{\epsilon}^{\varphi_i}$ to $\mathbf{Y}^{\varphi_i}$.

system (σ)

$\mathbf{x}_{\epsilon}^{\sigma}$		$\begin{bmatrix} x_{\epsilon_1}^{\sigma} & \ldots & x_{\epsilon_{\hat{\epsilon}}}^{\sigma} \end{bmatrix}$
$\boldsymbol{\Psi}^{\sigma}$		$\begin{bmatrix} T & p & \ldots & \psi_{\hat{\psi}}^{\sigma} \end{bmatrix}$
$\mathbf{X}^{\sigma}$		$\begin{bmatrix} \mathbf{x}_{\epsilon}^{\sigma} & \boldsymbol{\Psi}^{\sigma} \end{bmatrix}$
$\mathbf{Y}^{\sigma}$	$\tilde{\mathbf{Y}}^{\sigma}$	$\begin{bmatrix} \tilde{\mathbf{x}}_{\varphi}^{\sigma} & \tilde{\boldsymbol{\mu}}_{\epsilon}^{\sigma} & \tilde{\mathbf{T}}^{\sigma} & \tilde{\mathbf{P}}^{\sigma} & \begin{bmatrix} \tilde{\mathbf{Y}}^{\varphi_1} & \ldots & \tilde{\mathbf{Y}}^{\varphi_{\hat{\varphi}}} \end{bmatrix} \end{bmatrix}$

phase i (φ_i)

$\mathbf{Y}^{\varphi_i}$	$\tilde{\mathbf{Y}}^{\varphi_i}$	$\begin{bmatrix} \tilde{\mathbf{x}}_{\epsilon}^{\varphi_i} & \tilde{\mathbf{T}}^{\varphi_i} & \tilde{\mathbf{P}}^{\varphi_i} \end{bmatrix}$

Tolerances and Performance Measurement

$\Delta T^{\mathcal{D}}$	Temperature tolerance
$\Delta x_{\epsilon}^{\mathcal{D}}$	Composition tolerance
AF	Acceleration factor
Δt(direct)	Direct calculation elapsed time
Δt(accelerator)	Accelerated calculation elapsed time
$\mathrm{d}x_{\epsilon}^{\varphi_i}$	Phase i composition error
$\mathrm{d}x_{\varphi_i}^{\sigma}$	Phase i fraction error
$E\rho^{\sigma}$	Physical property error
$E\tau^{\sigma}$	Thermochemical property error

References

[1] W.A. Roos and J.H. Zietsman. Geometric acceleration of complex chemical equilibrium calculations – algorithm and application to two- and three-component systems. *CALPHAD: Computer Coupling of Phase Diagrams and Thermochemistry*, 77, 2021. doi: 10.1016/j.calphad.2022.102420.

[2] W.A. Roos and J.H. Zietsman. Accelerating complex chemical equilibrium calculations – a review. *CALPHAD: Computer Coupling of Phase Diagrams and Thermochemistry*, 77, 2021. doi: 10.1016/j.calphad.2021.102380.

[3] J.H. Zietsman and P.C. Pistorius. Modelling of an ilmenite-smelting dc arc furnace process. *Minerals Engineering*, 19:262–279, 2006. doi: 10.1016/j.mineng.2005.06.016.

[4] Ex Mente Technologies. Chemapppy, 2019. URL `https://www.ex-mente.co.za/chemapppy`.

[5] J.H. Zietsman. Efficient storage and recall of slag thermochemical properties for use in multiphysics models. In R.G. Reddy, P. Chaubal, P.C. Pistorius, and U. Pal, editors, *The 10th International Conference on Molten Slags, Fluxes and Salts*, pages 635–644, Seattle, USA, 2016. The Minerals, Metals and Materials Society. doi: 10.1007/978-3-319-48769-4_68.

[6] Guido Van Rossum and Fred L. Drake. *Python 3 Reference Manual*. CreateSpace, Scotts Valley, CA, 2009. ISBN 1441412697.

[7] Pauli Virtanen, Ralf Gommers, Travis E. Oliphant, Matt Haberland, Tyler Reddy, David Cournapeau, Evgeni Burovski, Pearu Peterson, Warren Weckesser, Jonathan Bright, Stéfan J. van der Walt, Matthew Brett, Joshua Wilson, K. Jarrod Millman, Nikolay Mayorov, Andrew R. J. Nelson, Eric Jones, Robert Kern, Eric Larson, C J Carey, İlhan Polat, Yu Feng, Eric W. Moore, Jake VanderPlas, Denis Laxalde, Josef Perktold, Robert Cimrman, Ian Henriksen, E. A. Quintero, Charles R. Harris, Anne M. Archibald, Antônio H. Ribeiro, Fabian Pedregosa, Paul van Mulbregt, and SciPy 1.0 Contributors. SciPy 1.0: Fundamental Algorithms for Scientific Computing in Python. *Nature Methods*, 17:261–272, 2020. doi: 10.1038/s41592-019-0686-2.

[8] J.H. Zietsman. *Interactions Between Freeze Lining and Slag Bath in Ilmenite Smelting*. PhD thesis, University of Pretoria, Pretoria, South Africa, 2004.

[9] M. Gous. An overview of the namakwa sands ilmenite smelting operations. *The South African Institute of Mining and Metallurgy*, 106:379–384, 2006.

[10] C.V.G.K. Murty, R. Upadhyay, and S. Asokan, editors. *Electro Smelting of Ilmenite for Production of TiO_2 Slag – Potential of India as a Global Partner*.

[11] P.C. Pistorius. Ilmenite smelting: The basics. *The Southern African Institute of Mining and Metallurgy*, 108:35–43, 2007. ISSN 2411-9717.

[12] X. Zhang, K. Jiao, J. Zhang, and Z. Guo. A review on low carbon emissions projects of steel industry in the world. *Journal of Cleaner Production*, 306, 2021. doi: 10.1016/j.jclepro.2021.127259.

[13] J.K. Pandit, M. Watson, and A. Qader. Reduction of greenhouse gas emission in steel production final report. publication number rpt20-6205. URL `https://www.resourcesregulator.nsw.gov.au/sites/default/files/2022-11/report-reduction-of-ghg-emissions-in-steel-industries.pdf`.

[14] A. Ghosh and A. Chatterjee. *Ironmaking and Steelmaking: Theory and Practice*. PHI Learning Private Limited, 2nd edition, 2008. ISBN 978-81-203-3289-8.

[15] J. Geiseler. Properties of iron and steel slags regarding their use. URL `https://www.pyrometallurgy.co.za/MoltenSlags2000/pdfs/207.pdf`.

[16] Federal Highway Administration U.S. Department of Transportation. User guidelines for waste and byproduct materials in pavement construction. URL `https://www.fhwa.dot.gov/publications/research/infrastructure/structures/97148/bfs1.cfm#`.

[17] A.J.B. Muwanguzi, A.V. Karasev, J.K. Byaruhanga, and P.J. Jo onsson. Characterization of chemical composition and microstructure of natural iron ore from muko deposits. *International Scholarly Research Network Materials Science*, 2012. doi: doi:10.5402/2012/174803.

[18] D.J.C. Taylor, D.C. Page, and P. Geldenhuys. Iron and steel in south africa. *The Southern African Institute of Mining and Metallurgy*, 88(3):73–95, 1988. doi: 10520/AJA0038223X_1819.

[19] R.J. Fruehan. *The Making, Shaping and Treating of Steel: Steelmaking and Refining Volume*. The AISE Steel Foundation, 11th edition. ISBN 978-0-930767-02-0.

[20] E. Belhadj, C. Diliberto, and A. Lecomte. Characterization and activation of basic oxygen furnace slag. *Cement and Concrete Composites*, 34:34–40, 2012. doi: 10.1016/j.cemconcomp.2011.08.012.

[21] T.S. Naidu, C.M. Sheridan, and L.D. van Dyk. Basic oxygen furnace slag: Review of current and potential uses. *Minerals Engineering*, 149, 2020. doi: 10.1016/j.mineng.2020.106234.

[22] M. Ruth. Steel production and energy. *Encyclopedia of Energy*, 5:695–706, 2004.